Radboud Repository

Radboud University Nijmegen

PDF hosted at the Radboud Repository of the Radboud University Nijmegen

The following full text is a publisher's version.

For additional information about this publication click this link.
http://hdl.handle.net/2066/149312

Please be advised that this information was generated on 2017-12-05 and may be subject to change.

QUANTUM CALCULATION OF INELASTIC CO COLLISIONS WITH H. II. PURE ROTATIONAL QUENCHING OF HIGH ROTATIONAL LEVELS

KYLE M. WALKER[1], L. SONG[2], B. H. YANG[1], G. C. GROENENBOOM[2], A. VAN DER AVOIRD[2], N. BALAKRISHNAN[3], R. C. FORREY[4], AND P. C. STANCIL[1]

[1] Department of Physics and Astronomy and Center for Simulational Physics, The University of Georgia, Athens, GA 30602, USA
[2] Theoretical Chemistry, Institute for Molecules and Materials, Radboud University, Heyendaalseweg 135, 6525 AJ Nijmegen, The Netherlands
[3] Department of Chemistry, University of Nevada Las Vegas, NV 89154, USA
[4] Department of Physics, Penn State University, Berks Campus, Reading, PA 19610, USA

ABSTRACT

Carbon monoxide is a simple molecule present in many astrophysical environments, and collisional excitation rate coefficients due to the dominant collision partners are necessary to accurately predict spectral line intensities and extract astrophysical parameters. We report new quantum scattering calculations for rotational deexcitation transitions of CO induced by H using the three-dimensional potential energy surface (PES) of Song et al. State-to-state cross sections for collision energies from 10^{-5} to $15,000 \, \mathrm{cm}^{-1}$ and rate coefficients for temperatures ranging from 1 to 3000 K are obtained for CO ($v = 0, j$) deexcitation from $j = 1$–45 to all lower j' levels, where j is the rotational quantum number. Close-coupling and coupled-states calculations were performed in full-dimension for $j = 1$–5, 10, 15, 20, 25, 30, 35, 40, and 45 while scaling approaches were used to estimate rate coefficients for all other intermediate rotational states. The current rate coefficients are compared with previous scattering results using earlier PESs. Astrophysical applications of the current results are briefly discussed.

Key words: ISM: molecules – molecular data – molecular processes – photon-dominated region (PDR)

1. INTRODUCTION

Carbon monoxide is the second most abundant molecule in the universe after molecular hydrogen and is found in a variety of astrophysical environments. The formation of CO in low-density interstellar clouds proceeds mainly through gas-phase chemical reactions involving H_2, and therefore detecting and measuring CO spectral lines is one way to trace the molecular interstellar medium (ISM) in the region. While H_2 rotational lines are difficult to observe from the ground, CO is more easily detected as its rovibrational transitions can be observed as absorption in the ultraviolet (UV) and near-infrared (NIR) and emission in the NIR, far-infrared (FIR), and submillimeter. The rotational energy level spacings of a diatomic molecule depend inversely on its moment of inertia, and the relatively large moment of inertia of CO compared to H_2 yields rotational levels with small energy separation. The lowest rotational transition of CO has a wavelength of ∼2.6 mm which gives an excitation temperature of just ∼5.5 K. Therefore, CO can be collisionally excited to high rotational levels in photon-dominated regions (PDRs), in shocks, and in other moderately energetic environments.

A number of CO pure rotational lines starting at $j = 14 \rightarrow 13$, where j is the rotational quantum number, have been detected with the Long-Wavelength Spectrometer (Clegg et al. 1996) aboard the *Infrared Space Observatory* (Kessler et al. 1996). These include the FIR spectra of all the lines up to $j = 39 \rightarrow 38$ in the carbon-rich circumstellar envelope IRC +10216 (Cernicharo et al. 1996), transitions up to $j = 25 \rightarrow 24$ in VY Canis Majoris and other oxygen-rich circumstellar envelopes (Polehampton et al. 2010), transitions up to $j = 24 \rightarrow 23$ from the carbon-rich planetary nebula NGC 7027 (Liu et al. 1996), and transitions up to $j = 19 \rightarrow 18$ of the Herbig Haro objects HH 52-53-54 and IRAS 12496-7650 in a nearby star-forming region (Nisini et al. 1996). The KOSMA 3 m and IRAM 30 m telescopes in

Switzerland and Spain, respectively, performed observations of the low-j transitions of CO in the Rosette Molecular Complex (Schneider et al. 1998), while the *Odin Orbital Observatory* (Nordh et al. 2003) detected $j = 5 \rightarrow 4$ emission from the PDR of Orion KL (Persson et al. 2007). More recently, the *Herschel Space Observatory* (Pilbratt et al. 2010) observed the $j = 9 \rightarrow 8$ line toward Monoceros R2 (Pilleri et al. 2012) and high-j CO lines in the NGC 1333 low-mass star-forming region (Yildiz et al. 2010) with the Heterodyne Instrument for the Far-Infrared (de Graauw et al. 2010). The Spectral and Photometric Imaging REceiver (Griffin et al. 2010) aboard *Herschel* has also probed the submillimeter molecular ISM of M82 from $j = 4 \rightarrow 3$ up to $j = 13 \rightarrow 12$ (Panuzzo et al. 2010).

The chemical and physical conditions where CO resides are deduced from observed spectral lines, but it is often not appropriate to assume local thermodynamic equilibrium (LTE) when modeling these regions. In low-density environments where the level populations routinely depart from LTE, collisional excitation rate coefficients with the dominant species—mainly H_2, H, He, and electrons—are necessary to accurately predict spectral line intensities. Although the effect of electron collisions is minor, the role of collisional excitation of CO by H, especially in environments such as diffuse molecular clouds (Goldsmith 2013) and cool mixed atomic and molecular hydrogen gas (Liszt 2006), cannot be neglected. Rate coefficient calculations for pure rotational excitation of the first 15 rotational levels of the He–CO system were performed by Cecchi-Pestellini et al. (2002) for the temperature range 5–500 K. Yang et al. (2010) calculated reliable H_2–CO rate coefficients for rotational transitions in CO induced by both para- and ortho-H_2 collisions for deexcitation from $j = 1$–40 to all lower j' levels for temperatures between 1 and 3000 K. Although the H–CO system has been studied extensively with the most recent rate coefficients reported by Yang et al. (2013),

there is unsatisfactory agreement between the results obtained upon the various potential energy surfaces (PESs).

The earliest analysis of H–CO collisions was performed by Chu & Dalgarno (1975), who used a short-range, semi-empirical potential joined with a long-range Buckingham potential to calculate cross sections via two close-coupling (CC) formulations. The resulting cross sections were found to be comparable to those of H_2–CO for small Δj. The Maxwellian-averaged rate coefficients were calculated for the temperature range of 5–150 K. The following year, quantal calculations were carried out by Green & Thaddeus (1976) over the same temperature range, but with a new semi-empirical potential and strikingly different results. These collisional rate coefficients were typically an order of magnitude smaller than those of Chu & Dalgarno (1975), and small Δj transitions, i.e., $|\Delta j| = 1$ or 2, were reported to have much larger rate coefficients when compared to large Δj transitions. The small magnitude of the H–CO rate coefficients obtained by Green & Thaddeus (1976) led to the neglect of H as a collider in CO emission modeling.

The next interaction PES for the H–CO system followed a more sophisticated level of theory using ab initio calculations for the surface (Bowman et al. 1986, hereafter called BBH). These calculations employed the Dunning & Hay (1971) valence double-zeta contractions of the Huzinaga (1971), (9s, 5p) sets of carbon- and oxygen-centered primitive Gaussians and used the (4s, 2s) contraction with a scale factor of 1.2 for hydrogen. Restricted Hartree–Fock calculations were carried out, followed by configuration interaction computations including all singly and doubly excited configurations. The resulting empirically corrected potential was used in dynamics calculations using a cubic spline interpolation. Subsequent coupled-channel scattering calculations were carried out on this PES by Lee & Bowman (1987) who first noticed the propensity for even-Δj transitions for inelastic scattering.

Another surface was constructed by Werner et al. (1995), hereafter WKS, to see if new experimental results could be more closely reproduced. The ab initio electronic structure calculations were performed with the MOLPRO program package (Werner et al. 2010) using the internally contracted multireference configuration interaction (icMRCI) method. Resonance energies and widths from the WKS surface agreed with experimental data (Keller et al. 1996), but striking differences were apparent in the collision cross sections obtained using the BBH and WKS surfaces (Green et al. 1996). The cross sections on the newer WKS surface, especially for low-j pure rotational transitions, yielded higher values than those calculated on the BBH surface. Balakrishnan et al. (2002) obtained similar results when they used both the BBH and the WKS surfaces to compute collisional rate coefficients for temperatures in the range 5–3000 K. The discrepancy in the CO ($j = 1 \rightarrow 0$) transition was the largest. However, Balakrishnan et al. (2002) performed explicit quantum-mechanical scattering calculations with the WKS PES for the first eight pure rotational transitions (using the CC framework) and first five vibrational levels (in the infinite order sudden approximation), and this complete set of rate coefficients has been extensively used in astrophysical models.

Shepler et al. (2007) revisited H–CO scattering by introducing two new rigid-rotor PESs and computing cross sections on each surface at collision energies of 400 and 800 cm^{-1}. One ab initio surface was calculated using the coupled cluster method with single and double excitations and a perturbative treatment of triple excitations [CCSD(T)] employing the frozen core approximation (Purvis & Bartlett 1982). Restricted Hartree–Fock orbitals were used for the open-shell calculations and the spin-restrictions were relaxed in the solution of the coupled cluster equations [R/UCCSD(T)] (Knowles et al. 1993). The other PES was computed using the complete active space self-consistent field (Knowles & Werner 1985) and icMRCI (Werner & Knowles 1988) method with the aug-cc-pVQZ basis set for H, C, and O by Woon & Dunning (1994) as implemented in the MOLPRO program. Their results for both potentials are more similar to Green & Thaddeus (1976) and it was recommended that the rate coefficients calculated by Balakrishnan et al. (2002) using the inaccurate WKS surface be abandoned. Based on this recommendation, astrophysical models using the overestimated rate coefficients should also be reexamined. The most recent set of H–CO calculations were performed by Yang et al. (2013) and extend the calculations of Shepler et al. (2007) on the MRCI rigid-rotor PES. State-to-state rotational deexcitation cross sections and rate coefficients from initial states $j = 1$–5 in the ground vibrational state to all lower j' levels were computed.

In this work, we report new quantum scattering calculations for rotational deexcitation transitions of CO induced by H using the three-dimensional (3D) interaction PES of Song et al. (2013). This 3D ab initio PES uses the spin-unrestricted open-shell single and double excitation coupled-cluster method with perturbative triples [UCCSD(T)] with molecular orbitals from restricted Hartree–Fock calculations (RHF). Electronic structure calculations were performed with the MOLPRO 2000 package (Werner et al. 2010) and 3744 interaction energies were included in the fit. When compared to previous PESs, the new 3D surface uses the most sophisticated level of theory and is the most accurate available for scattering calculations. State-to-state cross sections for collision energies from 10^{-5} to 15,000 cm^{-1} are computed for CO ($v = 0$, j) deexcitation from initial states $j = 1$–45 to all lower j' levels. While CC and coupled-states (CS) calculations, in full-dimension, are performed for $j = 1$–5, 10, 15, 20, 25, 30, 35, 40, and 45, scaling approaches are used to estimate the rate coefficients for all other intermediate rotational states. Rate coefficients for temperatures ranging from 1 to 3000 K are evaluated and compared with previous scattering results obtained on earlier surfaces. The astrophysical implications of new rotational deexcitation rate coefficients are illustrated.

2. COMPUTATIONAL APPROACH

We performed inelastic scattering calculations on the most current 3D PES of the H–CO complex in the ground state ($\widetilde{X}~^2A'$) (Song et al. 2013). Computations were carried out using the quantum mechanical CC method (Arthurs & Dalgarno 1960) for kinetic energies below 1000 cm^{-1}. From 1000 to 15,000 cm^{-1} the CS approximation of McGuire & Kouri (1974) was utilized. We treated hydrogen as a structureless atom and allowed the bond length to vary for CO. The full 3D surface is used in the calculations; at no point is the CO bond length fixed nor a rigid-rotor approximation made. The interaction potential was expressed as $V(R, r, \theta)$,
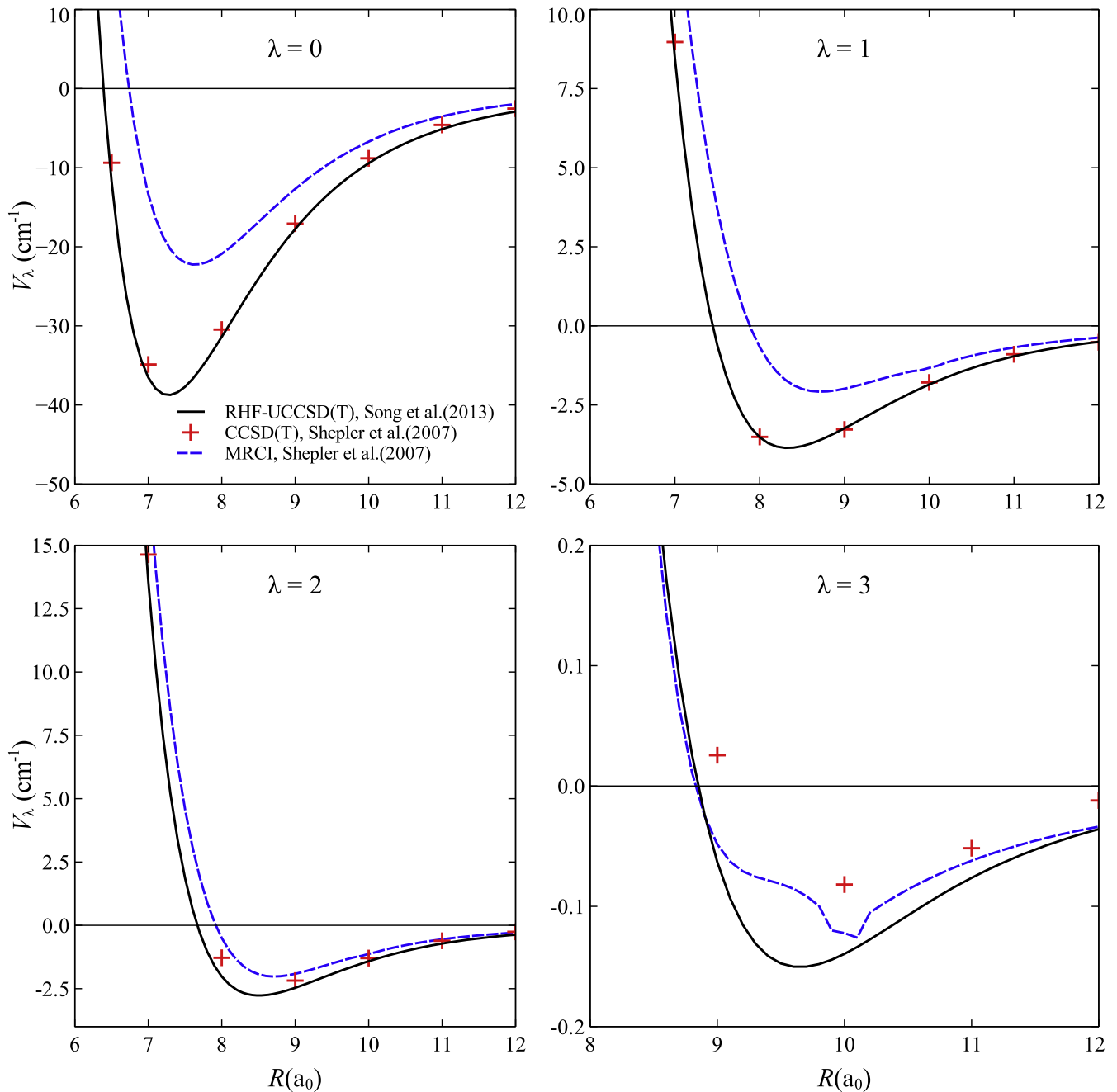
Figure 1. First four Legendre expansion terms $v_\lambda(R)$ near the van der Waals well of the H–CO PES with the CO intermolecular distance fixed at $r = 2.20$ a$_0$ for MRCI and the equilibrium bond length $r_e = 2.1322$ a$_0$ for the CCSD(T) and RHF-UCCSD(T) surfaces.

where r is the CO intramolecular distance, R the distance from the CO center of mass to the H nucleus, and θ the angle between the vector R and the CO bond axis, where linear C–O–H has an angle of zero degrees and $\theta = 180°$ for linear H–C–O. The potential was expanded according to

$$V(R, r, \theta) = \sum_{\lambda=0}^{\lambda_{max}} v_\lambda(R, r) P_\lambda(\cos \theta), \quad (1)$$

where P_λ are Legendre polynomials of order λ. The radial dependence of the potential used a 20-point Gauss–Hermite quadrature over r to represent CO stretching. The angular dependence of the potential was expanded to $\lambda_{max} = 20$ with a 22-point Gauss–Legendre quadrature.

The quantum-mechanical CC calculations were performed using the mixed-mode OpenMP/MPI version of the nonreactive scattering program MOLSCAT (Hutson & Green 1994) modified by Valiron & McBane (2008) and Walker (2013). The modified log-derivative Airy propagator of Alexander & Manolopoulos (1987) with variable step size was used to solve the coupled-channel equations. The propagation was carried out from $R = 1$ a$_0$ to a maximum distance of $R = 100$ a$_0$, where a$_0$ is the atomic unit of length (the Bohr radius). For calculations with initial state $j < 25$, the basis set included 31 rotational levels in the ground vibrational state of CO. For initial states $j \geqslant 25$ the basis sets included at least 5–10 closed rotational levels. Only pure rotational transitions within the $v = 0$ vibrational level are reported here. A convergence study
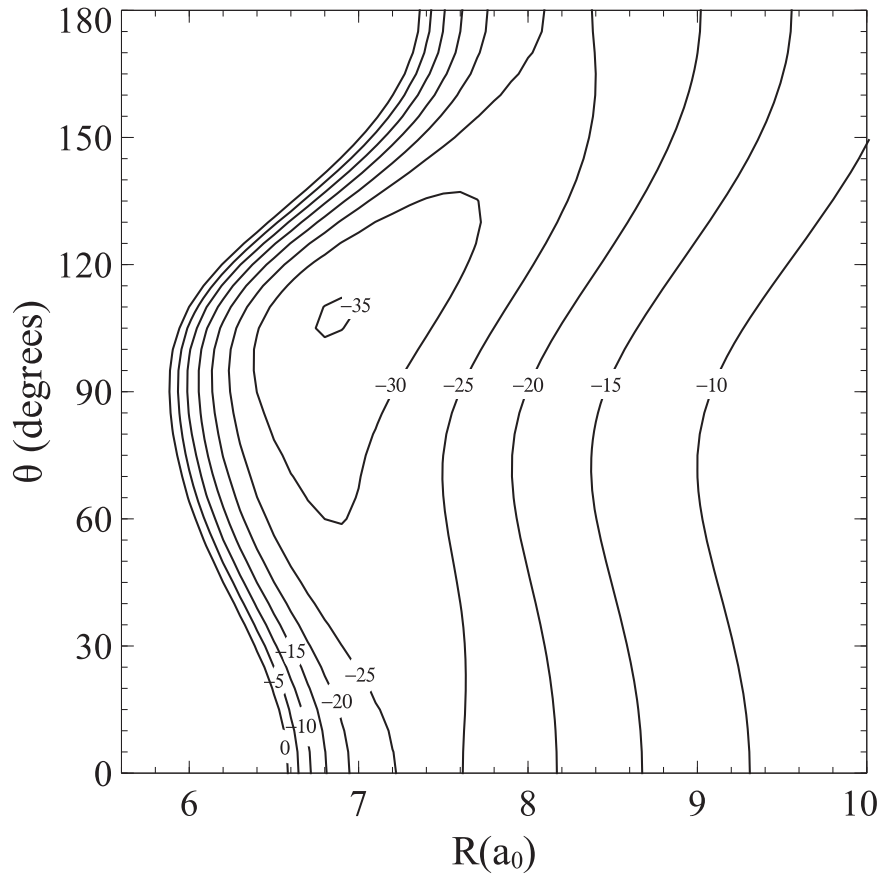
Figure 2. Long-range behavior of the interaction potential of Song et al. (2013) with V_{HCO} in cm^{-1} and r fixed at the equilibrium bond length $r_e = 2.1322$ a_0.

Table 1
Minima of the Interaction PESs

PES	$r_{CO}(a_0)$	$V_{min}(cm^{-1})$	$R(a_0)$	θ (degrees)
Global minimum:[a]				
MRCI[b]	2.20	−6934.052	3.01	145.5
CCSD(T)[b]	2.1322	−5817.161	3.00	144.7
RHF-UCCSD(T)[c]	2.1322	−5832.994	3.01	144.8
RHF-UCCSD(T)[c]	2.20	−7256.805	3.02	144.8
van der Waals minimum:				
MRCI	2.20	−19.934	7.21	110.8
CCSD(T)	2.1322	−34.677	6.87	108.1
RHF-UCCSD(T)	2.1322	−35.269	6.86	108.0
RHF-UCCSD(T)	2.20	−36.296	6.84	108.5

Notes.
[a] The term "global" is used loosely here since r_{CO} has been frozen at an unoptimized distance to ease direct comparison with the previous 2D surfaces.
[b] Shepler et al. (2007).
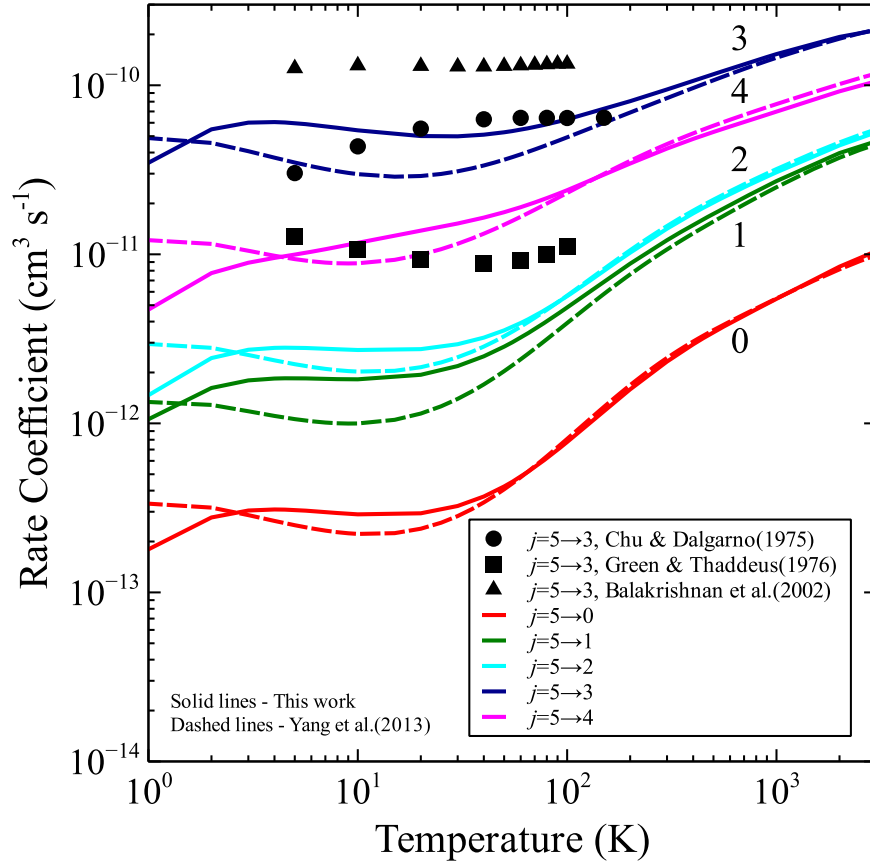[c] Song et al. (2013).

was performed with excited vibrational levels in the basis set, but the addition of higher vibrational levels yielded results within 2%. A sufficient number of angular momentum partial waves were included to ensure convergence to within 10% for the largest state-to-state cross sections. For the low energy range, 10^{-5}–10 cm^{-1}, maximum partial waves (J_{max}) was increased each decade resulting in the values 2, 4, 8, 12, 14, and 20 being added to the value of initial j, respectively, while

converged cross sections for energies from 10–49, 50–95, 100–900, 1000–9000, and 10,000–15,000 cm^{-1} were calculated by adding the values of 26, 30, 40, 50, and 60 to that of the initial state, respectively.

The degeneracy-averaged-and-summed integral cross section for a rotational transition from an initial state j to a final state j' in the CC formalism is given by

$$\sigma_{j \to j'}(E_j) = \frac{\pi}{(2j+1)k_j^2} \sum_{J=0}^{J_{max}} (2J+1)$$
$$\times \sum_{l=|J-j|}^{J+j} \sum_{l'=|J-j'|}^{J+j'} \left| \delta_{jj'}\delta_{ll'} - S_{jj'll'}^J(E_j) \right|^2, \qquad (2)$$

where j is the rotational angular momentum of the CO molecule, l is the orbital angular momentum of the collision complex, and $J = j + l$ is the total angular momentum. $S_{jj'll'}^J$ is an element of the scattering matrix, E_j is the relative kinetic energy of the initial channel, and $k_j = \sqrt{2\mu(E - \epsilon_j)}/\hbar$ is the wave-vector of the initial channel, where μ is the reduced mass of the H–CO system (0.97280 u), E is the total energy, ϵ_j is the rotational energy of CO, and $\hbar$ is the reduced Planck constant. The CS approximation, on the other hand, reduces the computation expense by neglecting the Coriolis coupling between different values of Ω, the projection of the angular momentum quantum number of the diatom along the body-fixed axis, and within this formalism the integral cross section

Figure 3. State-to-state pure rotational rate coefficients due to H collisions from initial state CO ($j = 5$) to indicated lower states j' from this work using the Song et al. (2013) PES, and from Yang et al. (2013) on the MRCI PES of Shepler et al. (2007). Previous rate coefficient calculations of Chu & Dalgarno (1975), Green & Thaddeus (1976), and Balakrishnan et al. (2002) on other surfaces are also shown for the dominant transition $j = 5 \rightarrow 3$.

is given by

$$\sigma_{j \rightarrow j'}(E_j) = \frac{\pi}{(2j+1)k_j^2} \sum_{J=0}^{J_{max}} (2J+1)$$
$$\times \sum_{\Omega=0}^{\Omega_{max}} (2 - \delta_{\Omega 0}) \left| \delta_{jj'} - S_{jj}^{J\Omega}(E_j) \right|^2, \quad (3)$$

where Ω_{max} is equal to 0, 1, 2, ..., max(J, j).

State-to-state cross sections for collision energies from 10^{-5} to 15,000 cm^{-1} were computed for CO ($v = 0, j$) deexcitation from initial state $j = 1$–5, 10, 15, 20, 25, 30, 35, 40, and 45 to all lower j' levels. Deexcitation rate coefficients ranging from 1 to 3000 K were obtained by averaging the cross sections over a Boltzmann distribution of collision energies,

$$k_{j \rightarrow j'}(T) = \left(\frac{8k_b T}{\pi \mu} \right)^{1/2} \frac{1}{(k_b T)^2} \int_0^\infty$$
$$\times \sigma_{j \rightarrow j'}(E_j) \exp(-E_j/k_b T) E_j dE_j, \quad (4)$$

where $\sigma_{j \rightarrow j'}$ is the state-to-state rotationally inelastic cross section, $E_j = E - \epsilon_j$ is the center of mass kinetic energy, and k_b is the Boltzmann constant.

3. RESULTS AND DISCUSSION

Before scattering calculations were carried out, we compared the RHF-UCCSD(T) 3D ab initio PES of Song et al. (2013) with the two-dimensional rigid rotor MRCI and CCSD(T)

surfaces of Shepler et al. (2007). The lower order Legendre terms of the RHF-UCCSD(T) PES agree well with the CCSD(T) terms; the similar high level of theory in both CCSD(T) calculations is expected to yield a more accurate potential than the lower-level MRCI calculations (see Figure 1). The higher-order λ-terms are typically small and decrease with λ. For example, for the RHF-UCCSD calculations shown in Figure 1, $v_3 \sim v_0/100$. Further, as the cross sections for a direct transition are driven by v_λ where $|\Delta j| = \lambda$, they are expected to decrease with $|\Delta j|$ and as a consequence the uncertainty in the cross sections are expected to increase with $|\Delta j|$, though multi-step transitions due to smaller v_λ terms will also contribute. The values of the Legendre expansion terms of the MRCI potential are all greater than those of the RHF-UCCSD(T) and CCSD(T) PESs. The feature seen in the MRCI results near $R = 10$ a_0 is due to the poor quality of fitting where the long-range and short-range regions are joined. Since the depth and location of the van der Waals well may strongly influence rotationally inelastic scattering, the behavior of the three interaction potentials was closely examined in the vicinity of the van der Waals well. Figure 2 shows a contour plot of the long-range behavior of the interaction potential of Song et al. (2013) with the CO bond length fixed at the equilibrium distance of $r_e = 2.1322$ a_0. The positions and values of the local and van der Waals minima on the three interaction PESs were calculated and are shown in Table 1. The van der Waals well of the MRCI potential is significantly different from that of the CCSD(T) and RHF-UCCSD(T) being both shallower and located at a larger internuclear distance. The differences in
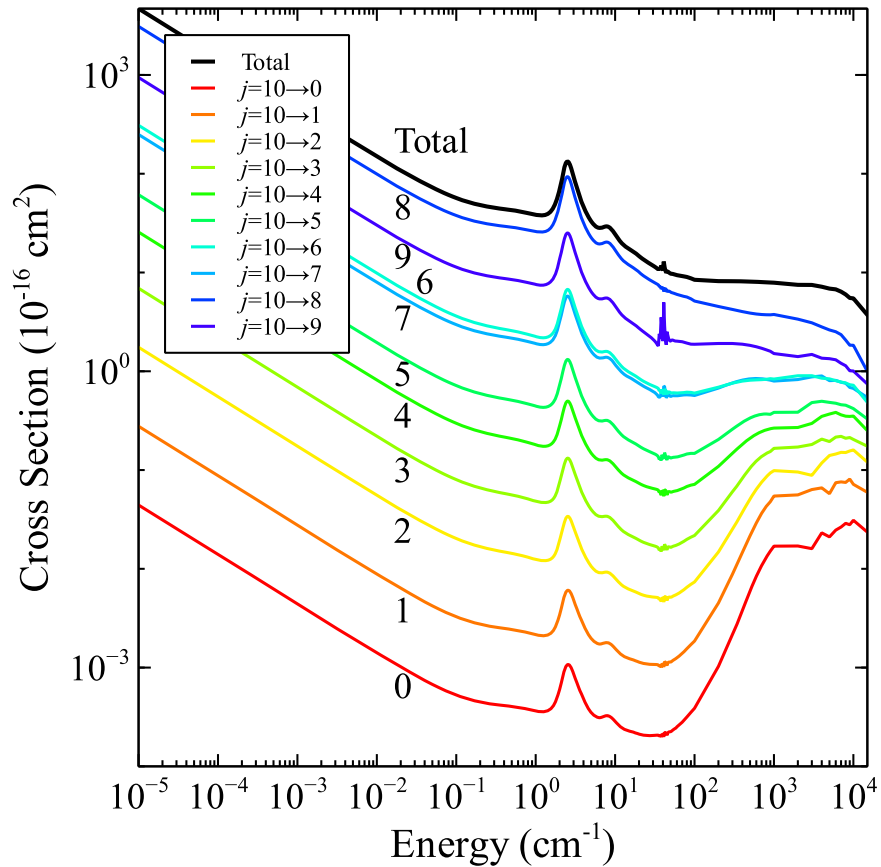
Figure 4. State-to-state pure rotational deexcitation cross sections due to H collisions from initial state CO ($j = 10$) to all lower states j'.

van der Waals well depth and anisotropies of the surfaces lead to differences in the scattering results.

Figure 3 shows state-to-state pure rotational H–CO rate coefficients from initial state CO ($j = 5$) to indicated lower states j'. The largest rate coefficients of CO ($5 \rightarrow 3$) as calculated by Chu & Dalgarno (1975), Green & Thaddeus (1976), and Balakrishnan et al. (2002) are shown. Rate coefficients from Yang et al. (2013) on the MRCI PES of Shepler et al. (2007) are also shown. The rate coefficients in this work agree well with those of Chu & Dalgarno (1975) and Yang et al. (2013). On average, rate coefficients of Green & Thaddeus (1976) are less than those of this work by around an order of magnitude, while the values from Balakrishnan et al. (2002) are around twice as much as ours. Although the CO ($5 \rightarrow 3$) transition is highlighted here, the results are typical for other state-to-state transitions as well.

Figures 4 and 5 present sample results from our computations of cross sections and rate coefficients, respectively, from initial state $j = 10$ to all final states j'. In general, the cross sections for $j' = 0$ are smallest and then increase with increasing j' up to the dominating transition where $|\Delta j| = |j' - j| = 2$ after which they decrease. Since CO is near-homonuclear, odd-Δj transitions are suppressed and the transitions follow an even-Δj propensity. At 1000 cm^{-1}, the difference between the CC and CS cross sections is less than $\sim 5\%$, except for the largest changes in Δj where the differences are typically $\sim 10\%$.

While the quenching from selected high rotational states is explicitly calculated, a zero-energy scaling technique is used to predict state-to-state rate coefficients for all intermediate states. Figure 6 shows the total quenching and state-to-state cross sections calculated at 10^{-5} cm^{-1} as a function of increasing j. The total quenching rate coefficient in the ultracold limit (collision energy of 10^{-5} cm^{-1}) is fairly constant for $j > 10$. Note that $\Delta j = -2$ dominates for low initial j, as expected, but at $j \sim 22$, $\Delta j = -1$ begins to dominate. From these ultracold state-resolved quenching rate coefficients, we estimated the rate coefficients for all temperatures following the procedure introduced in Yang et al. (2006), but modified here. The unknown rate coefficient for a transition from j to $j - \Delta j$ for any temperature T, given by $k(j, j - \Delta j; T)$, can be estimated based on the rate coefficients from calculated transitions for other initial rotational states, for example, larger j (i.e., above, j_A) or smaller j (i.e., below, j_B) ($k(j_A, j_A - \Delta j; T)$ and $k(j_B, j_B - \Delta j; T)$, respectively) and calculated ultracold ($T \sim 0$) rate coefficients for the transitions above, below, and the desired according to

$$
\begin{aligned}
k(j, j - \Delta j; T) &= k(j, j - \Delta j; T = 0) \\
&\times \frac{w_A k(j_A, j_A - \Delta j; T) + w_B k(j_B, j_B - \Delta j; T)}{w_A k(j_A, j_A - \Delta j; T = 0) + w_B k(j_B, j_B - \Delta j; T = 0)}.
\end{aligned}
\tag{5}
$$

Weights w_A and w_B for the calculated rate coefficients were determined by considering the change in initial j in the desired transition when compared to the states above and below
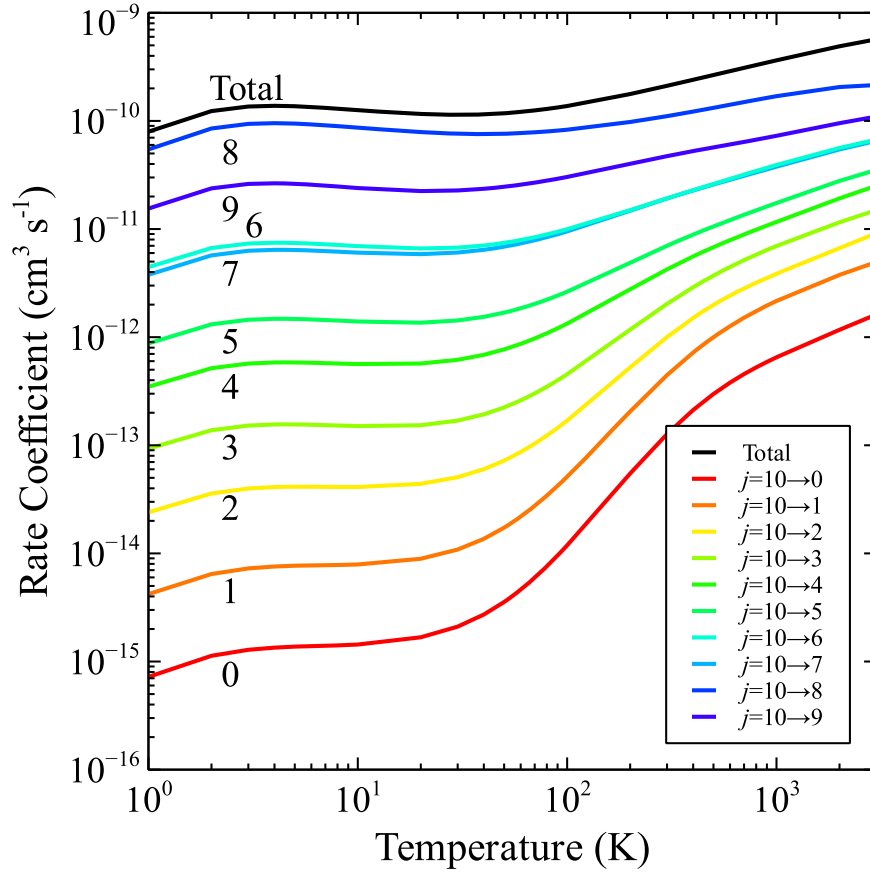
Figure 5. State-to-state pure rotational deexcitation rate coefficients due to H collisions from initial state CO ($j = 10$) to all lower states j'.
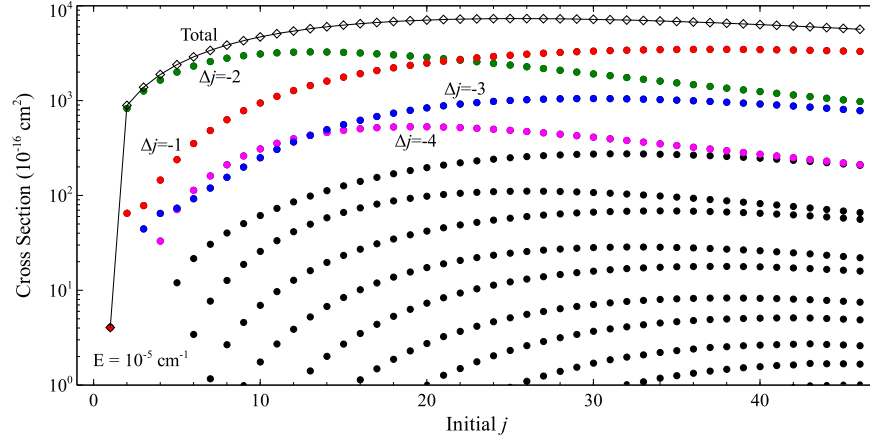
Figure 6. State-resolved cross sections at 10^{-5} cm^{-1} as a function of increasing j for the H–CO system. Circles indicate state-to-state cross sections while diamonds indicate total quenching cross sections. Each series (circles) correspond to different values of Δj, decreasing from the top at the far right as $\Delta j = -1, -2, -3, -4, ...$ (red, green, blue, magenta).

according to the equations

$$w_A = \frac{j - j_B}{j_A - j_B} \qquad w_B = \frac{j_A - j}{j_A - j_B}. \qquad (6)$$

For example, the predicted $j = 16$ rate coefficients used calculated transitions from $j = 20$ and $j = 15$ and weights $w_A = 0.2$ and $w_B = 0.8$. The cross sections at ultracold energies are easily calculated and simply multiplied by the velocity of the system (obtained from the kinetic

energy of the collision) to obtain the $T \sim 0$ rate coefficients. A comparison of this zero-energy scaling technique with explicit calculations is given in Figure 7 for initial state $j = 4$. The predicted rate coefficients agree well with the calculated values, although in this case transitions from $j = 3$ and $j = 5$ are equally weighted and a slight underestimations of the $j = 4 \rightarrow 2$ transition occurs. Given the high accuracy of the current PES, any uncertainty remaining in the computed cross section is likely due to
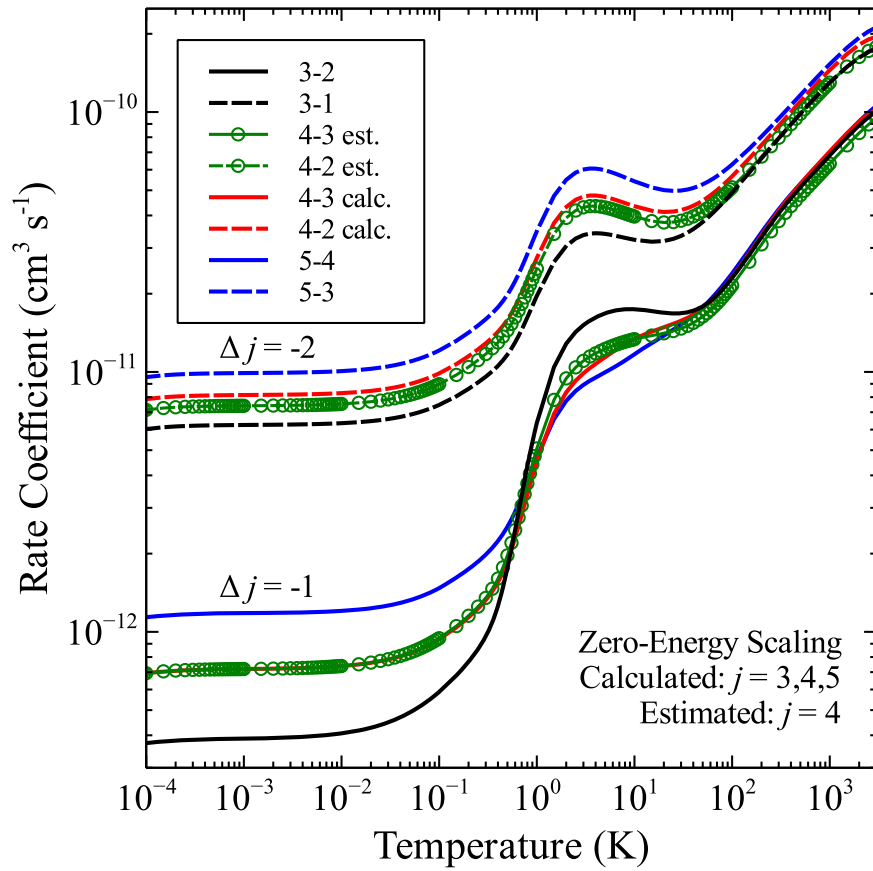
Figure 7. Comparison of the zero-energy scaling technique with explicit calculations of the largest deexcitation rate coefficients for initial state $j = 4$. Solid lines indicate $\Delta j = -1$ while dashed lines are $\Delta j = -2$. Initial states are: $j = 3$ (black), $j = 4$ estimated from Equation 5 (green with symbols), $j = 4$ explicitly calculated (red), and $j = 5$ (blue).
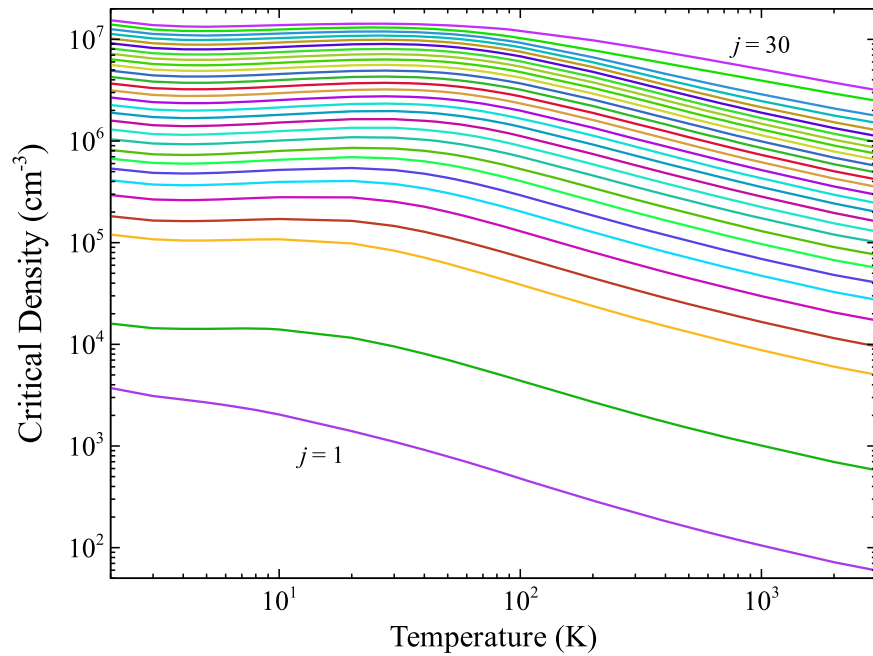
Figure 8. Critical densities for CO ($v = 0, j$) due to H collisions as a function of gas temperature T.

the adoption of the CS approximation, the truncation in the Legendre expansion of the PES to $\lambda_{max} = 20$ and the uncertainty in v_λ for large values of λ, and limited basis set sizes for collision energies above $1000\,cm^{-1}$. Otherwise, the interpolation formula introduces the largest source of uncertainty.

4. ASTROPHYSICAL APPLICATIONS

The cross sections and/or rate coefficients calculated in this work are available online.[5] These high-j pure rotational rate coefficients are especially useful as input data for codes developed to solve for level populations. One such code is RADEX (van der Tak et al. 2007), which can perform a non-LTE analysis of interstellar line spectra. The reliable rate coefficients calculated in this work also will help extract more accurate astrophysical conclusions from current models. Recently, Thi et al. (2013) modeled protoplanetary disks (PPDs) adopting the rate coefficients computed by Balakrishnan et al. (2002). These rate coefficients are based on an inaccurate interaction surface, so the conclusions of Thi et al. (2013) may be compromised. Furthermore, Thi et al. (2013) extrapolated the rate coefficients to higher temperatures. Our rate coefficients extend the range in temperature from previous studies up to 3000 K; therefore extrapolation in this case would not be necessary. It is expected that our reliable and comprehensive rate coefficients would lead to more accurate astrophysical models of PDRs, PPDs, and other molecular environments.

In the PPD models of Thi et al. (2013), they note that pure rotational transitions of CO probe the entire disk, while the warm inner regions are probed by rovibrational transitions. Further, the abundance of atomic hydrogen is high in the CO line-emitting region. In particular, it is typically greater than $10^6 \, \mathrm{cm}^{-3}$ throughout the disk, except near the mid-plane and at the disk surface. Assuming that H collisions and spontaneous emission, with transition probability $A_{j \to j'}$, dominate the CO rotational populations, the critical density for each rotational level j can be estimated following Osterbrock & Ferland (2006) with the relation

$$n_j^{\mathrm{cr}} = \frac{\sum_{j' < j} A_{j \to j'}}{\sum_{j' \neq j} k_{j \to j'}}, \tag{7}$$

and are displayed in Figure 8 (a similar figure for para-H_2 collisions can be found in Yang et al. 2010). Except near the inner disk where temperatures exceed 500 K and the density is greater than $10^8 \, \mathrm{cm}^{-3}$, levels for $j \gtrsim 15$ will not be in LTE. Infrared and UV-fluorescence pumping may also contribute resulting in supra-thermal CO rotational populations.

5. CONCLUSION

The 3D H–CO potential energy surface of Song et al. (2013) was used to perform quantum scattering calculations for rotational deexcitation transitions of CO induced by H. State-to-state cross sections for collision energies from 10^{-5} to $15{,}000 \, \mathrm{cm}^{-1}$ and rate coefficients for temperatures ranging from 1 to 3000 K were computed for CO pure rotational deexcitation. Not surprisingly, previous scattering results using a PES based on the CCSD(T) level of theory produced similar rate coefficients, but considered only low rotational excitation states. The MRCI surface of Shepler et al. (2007) with a less sophisticated level of theory also produced similar results as presented in Yang et al. (2013), while the scattering results of Balakrishnan et al. (2002) are deemed to be unreliable due to an inaccurate surface. The H–CO pure rotational rate coefficients presented here can be used to aid astrophysical modeling and they both extend the temperature range and angular momentum quantum number of reported H–CO rate coefficients. Further, while calculations of deexcitation from excited rovibrational levels have recently been performed (Song et al. 2015a, 2015b), experimental data on low-temperture rotational and vibrational inelastic rate coefficients would be highly desirable.

REFERENCES

Alexander, M. H., & Manolopoulos, D. E. 1987, JChPh, 86, 2044
Arthurs, A. M., & Dalgarno, A. 1960, RSPSA, 256, 540
Balakrishnan, N., Yan, M., & Dalgarno, A. 2002, ApJ, 568, 443
Bowman, J. M., Bittman, J. S., & Harding, L. B. 1986, JChPh, 85, 911
Cecchi-Pestellini, C., Bodo, E., Balakrishnan, N., & Dalgarno, A. 2002, ApJ, 571, 1015
Cernicharo, J., Barlow, M. J., González-Alfonso, E., et al. 1996, A&A, 315, L201
Chu, S.-I., & Dalgarno, A. 1975, RSPSA, 342, 191
Clegg, P. E., Ade, P. A. R., Armand, C., & Balutea, J.-P. 1996, A&A, 315, L38
de Graauw, T., Helmich, F. P., Phillips, T. G., et al. 2010, A&A, 518, L6
Dunning, T. H., Jr., & Hay, P. J. 1971, in Methods in Electronic Structure Theory, ed. H. F. Schaefer, III (New York: Plenum), 1
Goldsmith, P. F. 2013, ApJ, 774, 134
Green, S., Keller, H.-M., Schinke, R., & Werner, H.-J. 1996, JChPh, 105, 5416
Green, S., & Thaddeus, P. 1976, ApJ, 205, 766
Griffin, M. J., Abergel, A., Abreu, A., et al. 2010, A&A, 518, L3
Hutson, J. M., & Green, S. 1994, MOLSCAT Computer Code, version 14, Distributed by Collaborative Computational Project No. 6 of the Engineering and Physical Sciences Research Council (UK)
Huzinaga, S. 1971, Approximate Atomic Wave Functions. I, Chemistry Report (Edmonton: Univ. Alberta)
Keller, H.-M., Floethmann, H., Dobbyn, A. J., et al. 1996, JChPh, 105, 4983
Kessler, M. F., Steinz, J. A., Anderegg, M. E., et al. 1996, A&A, 315, 27
Knowles, P. J., Hampel, C., & Werner, H.-J. 1993, JChPh, 99, 5219
Knowles, P. J., & Werner, H.-J. 1985, CPL, 115, 259
Lee, K.-T., & Bowman, J. M. 1987, JChPh, 86, 215
Liszt, H. S. 2006, A&A, 458, 507
Liu, X.-W., Barlow, M. J., Nguyen, R. Q., et al. 1996, A&A, 315, L257
McGuire, P., & Kouri, D. J. 1974, JChPh, 60, 2488
Nisini, B., Lorenzetti, D., Cohen, M., et al. 1996, A&A, 315, L321
Nordh, H. L., von Schéele, F., Frisk, U., et al. 2003, A&A, 402, L21
Osterbrock, D. E., & Ferland, G. J. 2006, Astrophysics of Gaseous Nebulae and Active Galactic Nuclei (2nd ed.; Sausalito: Univ. Science)
Panuzzo, P., Rangwala, N., Rykala, A., et al. 2010, A&A, 518, L37
Persson, C. M., Olofsson, A. O. H., Koning, N., & Bergman, P. 2007, A&A, 476, 807
Pilbratt, G. L., Riedinger, J. R., Passvogel, T., et al. 2010, A&A, 518, L1
Pilleri, P., Fuente, A., Cernicharo, J., et al. 2012, A&A, 544, A110
Polehampton, E. T., Menten, K. M., van der Tak, F. F. S., & White, G. J. 2010, A&A, 510, A80
Purvis, G. D., & Bartlett, R. J. 1982, JChPh, 76, 1910
Schneider, N., Stutzki, J., Winnewisser, G., & Block, D. 1998, A&A, 335, 1049
Schoier, F. L., van der Tak, F. F. S., van Dishoeck, E. F., & Black, J. H. 2005, A&A, 432, 369
Shepler, B. C., Yang, B. H., Dhilip Kumar, T. J., et al. 2007, A&A, 475, L15
Song, L., Balakrishnan, N., van der Avoird, A., et al. 2015a, JChPh, 142, 204303
Song, L., Balakrishnan, N., Walker, K. M., et al. 2015b, ApJ, submitted
Song, L., van der Avoird, A., & Groenenboom, G. C. 2013, JPCA, 117, 7571

---

[5] Rate coefficient data in the Leiden Atomic and Molecular Database (LAMDA, Schoier et al. 2005) format, as well as cross section data can be obtained at www.physast.uga.edu/amdbs/excitation/.

Thi, W. F., Kamp, I., Woitke, P., et al. 2013, A&A, 551, A49

Valiron, P., & McBane, G. C. 2008, Mixed MPI and OpenMP extension of the MOLSCAT v14 package

van der Tak, F. F. S., Black, J. H., Schöier, F. L., et al. 2007, A&A, 468, 627

Walker, K. M. 2013, VRRMM Vibrational/Rotational Rich Man's MOLSCAT v3.1

Werner, H.-J., Bauer, C., Rosmus, P., et al. 1995, JChPh, 102, 3593

Werner, H.-J., & Knowles, P. J. 1988, JChPh, 89, 5803

Werner, H.-J., Knowles, P. J., Almlöf, J., et al. 2010 MOLPRO is a package of ab initio programs. http://www.molpro.net

Woon, D. E., & Dunning, T. H., Jr. 1994, JChPh, 100, 2975

Yang, B. H., Perera, H., Balakrishnan, N., et al. 2006, JPhB, 39, S1229

Yang, B. H., Stancil, P. C., Balakrishnan, N., & Forrey, R. C. 2010, ApJ, 718, 1062

Yang, B. H., Stancil, P. C., Balakrishnan, N., et al. 2013, ApJ, 771, 49

Yildiz, U. A., van Dishoeck, E. F., Kristensen, L. E., et al. 2010, A&A, 521, L40